Mode sequence, frequency change of nonsoft phonons, and LO-TO splitting in strained tetragonal $BaTiO_3$

Aldo Raeliarijaona and Huaxiang Fu
Department of Physics, University of Arkansas, Fayetteville, Arkansas 72701, USA
(Received 4 June 2015; published 4 September 2015)

Ultraviolet Raman spectroscopy revealed the existence of an unusual large-frequency shift occurring to a *nonsoft* mode of $E(TO_4)$ when $BaTiO_3$ is strained to a $SrTiO_3$ substrate [D. Tenne *et al.*, Science **313**, 1614 (2006)]. It raised two interesting questions: (i) whether there are other nonsoft modes that possess similar or even larger strain-induced frequency shifts and (ii) how the mode sequence is altered by these shifts in frequency. Note that mode sequence is also pivotal in correctly indexing and assigning the spectroscopy peaks observed in all Raman experiments. By mapping out the evolutions of individual phonon modes as a function of strain using first-principles density functional perturbation calculations, we determine the mode sequence and strain-induced phonon frequency shifts in prototypical $BaTiO_3$. Our study reveals that the mode sequence is drastically different when $BaTiO_3$ is strained to $SrTiO_3$ compared to that in the unstrained structure, caused by multiple mode crossings. Furthermore, we predict that three other nonsoft modes, $A_1(TO_2)$, $E(LO_4)$, and $A_1(TO_3)$, display even larger strain-induced frequency shifts than $E(TO_4)$. The strain responses of individual modes are found to be highly mode specific, and a mechanism that regulates the magnitude of the frequency shift is provided. As another key outcome of this study, we tackle a long-standing problem of LO-TO splitting in ferroelectrics. A rigorous definition for the LO-TO splitting is formulated, which allows this critical quantity to be calculated quantitatively. The definition immediately reveals a new finding; that is, a large LO-TO splitting not only exists for $E(LO_4)$, which is previously known and originates from a soft mode, it also occurs for a nonsoft $A_1(LO_3)$ mode. The LO-TO splitting is shown to decrease drastically with compressive strain, and this decrease cannot be explained by the Born effective charges and high-frequency dielectric constants.

DOI: 10.1103/PhysRevB.92.094303 PACS number(s): 63.20.−e, 77.84.−s, 77.80.bn

I. INTRODUCTION

A breakthrough was made in probing the lattice dynamics in nanoscale ferroelectrics (FE) [1–3] by using *ultraviolet* (UV) Raman spectroscopy rather than conventional Raman spectroscopy. Conventional Raman spectroscopy uses *visible* light as the probing source [4] and works poorly for FE thin films since visible light, with its energy being much smaller than the band gaps of FE oxides, is weakly absorbed by thin films and will penetrate deeply into substrates, leading to large unwanted signals from substrates and thus a low resolution. In fact, the signal of visible-light Raman spectroscopy largely comes from the vibrations of the substrate, not from FE thin films. In contrast, the UV Raman, utilizing UV light with an energy larger than the band gaps of oxides, can be absorbed strongly by the FE thin films and thus can reveal the phonon structure of thin films with high resolution. Indeed, using UV Raman, multiple sharp peaks were clearly observed in $BaTiO_3/SrTiO_3$ superlattices epitaxially grown on a $SrTiO_3$ substrate [1,2].

Furthermore, interesting phonon physics was revealed [1]. For instance, a new and pronounced Raman peak was observed at frequency 540 cm^{-1} and was assigned as the transverse TO_4 mode originating from the strained $BaTiO_3$ [1]. However, in bulk $BaTiO_3$, the frequency of the TO_4 mode is merely 486 cm^{-1} (Ref. [5]). Although it is known that strain may cause a large-frequency shift in the soft mode, note that TO_4 is not a soft mode, however. A very large strain-induced frequency shift that occurs in a nonsoft mode is interesting itself. It further raises other intriguing questions: (i) What is the origin of the drastic frequency shift? (ii) Are there other nonsoft modes that may also exhibit large-frequency shifts that have not been detected in experiments?

Previously, there were many important works on the lattice dynamics in ferroelectrics, yielding critical understanding of the structural instability [6,7], the characteristic difference in phonon dispersion among different materials [8], phonons in composition-modulated FE superlattices [9], and finite electric-field-induced phonon hardening in incipient ferroelectrics [10,11]. Most of these studies paid attention to the behaviors of soft modes in the high-symmetry *nonpolar* phase, namely, the phase before ferroelectric transition occurs. In contrast, relatively less attention is given to the *polar* phase [12] and to the nonsoft phonon modes.

The experimental advance [1–3] also brings up another issue of broad interest, namely, how the sequence of phonon modes is altered by external conditions. Sequencing of phonon modes, namely, the ordering of vibration modes according to frequencies, is of fundamental relevance for unveiling the interatomic interaction in solids [13] because the sequence is determined by the microscopic nuclei-nuclei, nuclei-electron, and electron-electron interactions. In contrast to a *single* mode, the mode sequencing reflects collectively the behaviors of a *group* of modes. Since different modes respond to the external conditions (such as pressure, strain, and electric field) in different manners, it is nontrivial to determine how the mode sequence alters with external conditions. Determination of mode sequencing is also of practical importance since in infrared or Raman experiments this sequence is much needed in order to correctly assign phonon modes to individual peaks and to determine the origin of these peaks [4]. This knowledge is particularly relevant when the mode sequence under the

ambient condition is, after the external condition has changed, no longer valid.

Owing to the facts that (i) ferroelectric properties are sensitive to lattice dynamics [6–9,14] and (ii) ferroelectrics possess a myriad of technological applications in dielectric capacitors [15,16], field-effect transistors [17], electrical-caloric energy conversion [18], piezoelectric devices and transducers [19–23], and nonvolatile ferroelectric random access memory [24], studying phonon properties in ferroelectrics is thus very important. Interest in ferroelectrics also arises from the fundamental concepts these materials can bring attention to, such as the origin of ferroelectricity [25,26], the modern theory of polarization [27,28], the theory of phase transitions [29,30], etc.

Another subject of profound interest in FEs is the LO-TO splitting. Transverse-optic (TO) modes interact with light, which is a key process that determines optical properties [13]. On the other hand, longitudinal-optic (LO) modes interplay with electric fields, determining the dielectric responses of solids [13]. The LO and TO modes are thus of key importance in both optical and dielectric properties. Further, the LO and TO modes are also critical in testing the fundamental $2n-1$ sum rule [31]. Moreover, the LO-TO splitting arises from the long-range Coulomb interaction, manifesting the influence of this interaction on the lattice dynamics and the origin of anomalous Born effective charge [32,33].

A long-standing problem inhibits the *quantitative* study of the LO-TO splitting, however. That is, the splitting has not been fundamentally well defined. As have been realized by Zhong *et al.* in a seminal work [32], it is generally *not* possible to find a one-to-one correspondence between a LO mode and a TO mode. In fact, when lattice vibrations interact with electric fields via the long-range Coulomb interaction, more than one TO mode may contribute simultaneously, and all of them significantly, to form a single LO mode as a result of the strong mode mixing caused by the Coulomb interaction. Here we give a concrete example to illustrate this spread mode mixing. We consider $BaTiO_3$ at a compressive strain of -2.5%. By quantitative mode projection, our first-principles calculations show that the $E(LO_4)$ mode at frequency $\omega = 735$ cm^{-1} has contributions from five TO modes with the contribution weights at 7%, 23%, 21%, 8%, and 40%, revealing that the contributions are indeed widespread and there is no dominant one. This mode mixing is fundamental and cannot be avoided. As a consequence, an attempt to define the LO-TO splitting as the frequency difference between one LO mode and one TO mode cannot be justified. The lack of quantitative study of the LO-TO splitting hampers efforts to obtain insightful knowledge about this important quantity. It also prevents us from investigating how the splitting may be quantitatively tuned by external conditions such as epitaxial strain and electric field.

The purposes of this paper are fourfold: (i) to explain the origin of the large-frequency shift of the nonsoft TO_4 mode observed in the UV Raman experiments and, one step further, to determine which modes are susceptible and which modes react less to the epitaxial strain, (ii) to reveal how the sequencing of phonon modes can be significantly changed by strain and thus why the mode sequence at ambient conditions should not be used to assign the peaks observed in strained FEs, (iii) to show that the LO-TO splitting can be rigorously defined, which paves the way to quantitatively study this important quantity, and (iv) to determine whether there are any other modes that exhibit large LO-TO splittings besides the soft TO mode.

This paper is organized as follow. In Sec. II we describe the calculation methods and theories pertinent to the vibrations in solids, and then in Sec. III we present the calculation results along with some key theoretical formulations for analysis. A summary in Sec. IV concludes the paper. Other useful results on the phonon displacements and infrared (IR) intensities are given in the Appendix.

II. THEORETICAL METHODS

Structural optimization. We consider tetragonal $BaTiO_3$ with $P4mm$ symmetry. Total energy, atomic forces, and structural optimization are determined using the density functional theory (DFT) within the local-density approximation [34] (LDA) via QUANTUM ESPRESSO [35,36]. Troullier-Martins pseudopotentials [37] are used to mimic the interaction between valence electrons and inert core electrons. Ti $3s$ and $3p$ semicore states are treated as valence states [38]. The energy cutoff for wave-function expansions is 95 Ry. Both cell parameters and atomic positions are optimized for a given in-plane strain, with the force threshold set below 10^{-5} Ry/bohr. The biaxial η strain is enforced by changing the in-plane lattice constant a as $\eta = \frac{a-a_0}{a_0}$, where a_0 is the in-plane lattice constant of $BaTiO_3$ at equilibrium. A negative η means that the strain is compressive. We find for unstrained $BaTiO_3$ $a_0 = 3.93$ Å and $c/a = 1.007$, which are close to the values in other calculations (for instance, $a_0 = 3.945$ Å and $c/a = 1.009$ in Ref. [39]).

Phonon structure. Phonon frequencies and eigenvectors are determined by the density functional perturbation theory (DFPT) [40–42]. Vibration of atoms leads to the deformation potential $\Delta V(\mathbf{r}) = \sum_{l,i}[V(\mathbf{r}-\mathbf{R}_l-\mathbf{t}_i-\mathbf{u}_i) - V(\mathbf{r}-\mathbf{R}_l-\mathbf{t}_i)]$, where $\mathbf{t}_i$ and $\mathbf{u}_i$ are the equilibrium ionic position and atomic displacement of atom i, respectively; $\mathbf{R}_l$ is the lattice vector for cell l. By treating ΔV as perturbation, the response of electron density $\Delta n(\mathbf{r}) = 4\mathrm{Re}\sum_n^{N/2} \psi_n^*(\mathbf{r})\Delta\psi_n(\mathbf{r})$ is determined by solving the Sternheimer equation [40],

$$(H_{scf} - \varepsilon_n)|\Delta\psi_n\rangle = -(\Delta V_{scf} - \Delta\varepsilon_n)|\psi_n\rangle \ , \qquad (1)$$

where H_{scf} is the Kohn-Sham Hamiltonian, ε_n is the single-particle eigenvalue of H_{scf}, and $\Delta V_{scf}(\mathbf{r}) = \Delta V(\mathbf{r}) + e\int \frac{\Delta n(\mathbf{r}')}{|\mathbf{r}-\mathbf{r}'|}\,dr' + \frac{dv_{xc}(n)}{dn}|_{n=n(\mathbf{r})}\Delta n(\mathbf{r})$ is the self-consistent perturbation potential.

With Δn and $\Delta\psi$, other important quantities such as the change in the electric polarization $\Delta\mathbf{P}$, the Born effective charges $\mathbf{Z}^*$, and the dielectric tensor $\boldsymbol{\epsilon}$ can be calculated, respectively, as $\Delta\mathbf{P} = \sum_i z_i e\mathbf{u}_i - \frac{e}{V}\int_V \mathbf{r}\Delta n(\mathbf{r})\,d\mathbf{r}$, $(Z_i^*)_{\alpha\beta} = \frac{\Omega}{e}\frac{\partial P_\alpha}{\partial u_i^\beta(\mathbf{q}=0)}|_{\mathbf{E}=0}$, and $\epsilon_{\alpha\beta}^\infty = \delta_{\alpha\beta} + 4\pi\frac{\partial P_\alpha}{\partial E_\beta}|_{\mathbf{u}_i(\mathbf{q}=0)}$, where α and β are the direction indices and Ω is the unit-cell volume.

TABLE I. Born effective charges and high-frequency dielectric constants for unstrained $BaTiO_3$. O2 is the apical oxygen atom beneath Ti along the tetragonal c axis.

Quantity	Present work	Other work [44]
Z^*_{xx}(Ba)	2.77	2.73
Z^*_{zz}(Ba)	2.81	2.81
Z^*_{xx}(Ti)	7.11	7.04
Z^*_{zz}(Ti)	6.54	5.97
Z^*_{xx}(O1)	−5.56	−5.60
Z^*_{zz}(O1)	−2.05	−2.15
Z^*_{xx}(O2)	−2.09	−2.02
Z^*_{zz}(O2)	−5.07	−4.84
ϵ^∞_{xx}	6.54	6.48
ϵ^∞_{zz}	6.07	5.84

Nonanalytic contribution at $\mathbf{q} = 0$. When dealing with the long-wavelength phonons with wave vector $\mathbf{q}$ at the zone center, the interatomic force constant (IFC) matrix can be divided into analytic and nonanalytic contributions $C^{\alpha\beta}_{ij} = C^{a,\alpha\beta}_{ij} + C^{na,\alpha\beta}_{ij}$, where i and j are atomic indices. The nonanalytic part takes the form [43] $C^{na,\alpha\beta}_{ij} = \frac{4\pi}{\Omega} e^2 \frac{(\mathbf{q}\cdot\mathbf{Z}^*_i)_\alpha (\mathbf{q}\cdot\mathbf{Z}^*_j)_\beta}{\mathbf{q}\cdot\boldsymbol{\epsilon}^\infty\cdot\mathbf{q}}$. Note that C^{na} is not diagonal and will often cause strong mixing among different modes. At $\mathbf{q} = 0$, the nonanalytic contribution can be calculated by allowing $\mathbf{q}$ to approach the Brillouin zone center from a chosen direction. This nonanalytic contribution leads to the difference in frequency between the LO phonon ($\mathbf{u}\|\mathbf{q}$) and the TO phonon ($\mathbf{u}\perp\mathbf{q}$) due to the strong interaction between ions and displacement-induced electric field [4,13].

III. RESULTS AND DISCUSSION

Before we present our main results for strained $BaTiO_3$, it is important to examine the dielectric and phonon properties at zero strain since they are used as reference for the strained cases. The Born effective charges Z^* and high-frequency dielectric constant ϵ^∞ are given in Table I, and the phonon frequencies of the zone-center modes are in Table II. We see that Z^* and ϵ^∞ obtained in our calculations are in good agreement with others [44], and so are the phonon frequencies [5,45]. The slight difference between our results and those of Ref. [44] in Table I is because the authors of Ref. [44] performed their calculations using the experimental value of the lattice constant.

The normal modes in tetragonal $BaTiO_3$ are $5E \bigoplus 4A_1 \bigoplus B_1$, labeled according to the irreducible representations of the crystallographic space group $P4mm$. E modes are doubly degenerate; these modes vibrate along the ab plane on which the biaxial strain is applied. A_1 and B_1 modes are singly degenerate and vibrate along the c axis perpendicular to the directions of applied biaxial strain. Since the tetragonal phase is not the most stable phase for $BaTiO_3$ (the rhombohedral phase is), obviously, there is one soft mode, $E(TO_1)$, in Table II, as it should be. The atomic vibration directions and amplitudes are shown in the Appendix for each mode.

According to their vibration patterns in the Appendix, the modes can be categorized as (i) Slater modes, in which Ti and O atoms vibrate opposite each other without significantly involving Ba, such as $E(TO_1)$, $E(LO_4)$, $A_1(TO_2)$, and $A_1(LO_3)$, (ii) Last modes, where Ti and O vibrate in the same direction but opposite Ba, such as $E(TO_2)$, $E(LO_1)$, $A_1(TO_1)$, and $A_1(LO_1)$, (iii) the Axe mode, where the O atoms on one plane (not necessarily the base plane) vibrate opposite that of the O atom out of the plane, e.g., $E(TO_4)$ and $A_1(TO_3)$, (iv) the Axe + Ti mode, whose vibration pattern resembles the Axe mode but involving Ti, e.g., $E(LO_3)$ and $A_1(LO_2)$, and (v) the O-plane distortion mode, where the O atoms on one plane move in opposite directions, e.g., $E(TO_3)$, $E(LO_2)$, and B_1.

TABLE II. Frequencies of the phonon modes at the zone center in zero-strained $BaTiO_3$.

ω (cm^{-1})	Present work	Other theory [45]	Experiments [5]
$E(TO_1)$	–78	–79	36
$A_1(TO_1)$	178	190	170
$E(LO_1)$	180	188	180
$E(TO_2)$	183	192	180
$A_1(LO_1)$	186	195	185
$A_1(TO_2)$	211	237	270
B_1	296	301	305
$E(LO_2)$	300	302	305
$E(TO_3)$	300	302	305
$E(LO_3)$	462	462	463
$A_1(LO_2)$	465	465	475
$E(TO_4)$	480	487	486
$A_1(TO_3)$	497	507	520
$E(LO_4)$	678	701	715
$A_1(LO_3)$	697	721	720

A. Mode sequence in strained $BaTiO_3$

Phonon frequencies at Γ in $BaTiO_3$ under six different in-plane strains are shown in the inset of Fig. 1. Note that only discrete symbols such as those in the inset of Fig. 1 are the results directly obtained from calculations. With these discrete symbols alone, it is hard to figure out which mode at $\eta = -2.5\%$ corresponds to which mode at $\eta = 0$ since strain often gives rise to frequency crossings due to strong mixing between different modes. Furthermore, in the inset of Fig. 1, many modes have nearly the same frequency, and keeping track of the strain-induced evolution for these modes is nontrivial. As a consequence, the important knowledge of how individual phonon modes evolve with strain and how the mode sequence changes with strain is unclear.

To solve this problem and to obtain valuable insight into the phonon evolution with strain, we use an approach based on mode projection. Let $|\epsilon^{i\alpha}_n(\eta)\rangle$ be the phonon eigenvector of the nth mode at strain η; $|\epsilon^{i\alpha}_n(\eta)\rangle$ is related to the phonon displacement $|u^{i\alpha}_n(\eta)\rangle$ by $|\epsilon^{i\alpha}_n(\eta)\rangle = \sqrt{M_i}|u^{i\alpha}_n(\eta)\rangle$, where i is the atom index, α is the direction index, and M_i is the mass of atom i. The eigenvectors satisfy the orthonormality condition $\sum_{i\alpha}\langle\epsilon^{i\alpha}_m(\eta)|\epsilon^{i\alpha}_n(\eta)\rangle = \delta_{mn}$. Using the vibration eigenvectors at η_1 as bases, one can expand the eigenvectors at η_2 as

$$\epsilon^{i\alpha}_n(\eta_2) = \sum_m p_{mn}\,\epsilon^{i\alpha}_m(\eta_1)\,, \tag{2}$$

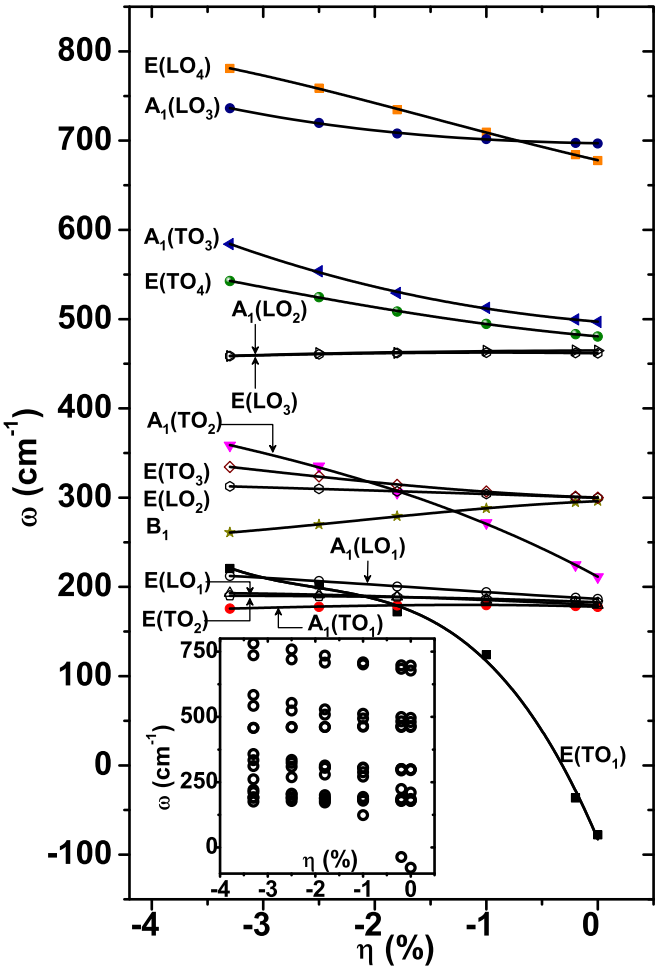

FIG. 1. (Color online) Phonon frequencies at Γ as a function of epitaxial strain. The acoustic phonons at Γ are trivial and hence are omitted from this plot. The nonanalytic C^{na} matrix is calculated with **q** approaching the zone center along the [001] direction for A_1(LO) modes and along the [100] direction for E(LO) modes. The inset shows the mode frequencies directly obtained from the DFPT calculations before applying the mode projection.

where $p_{mn} = \sum_{i\alpha} \langle \epsilon_m^{i\alpha}(\eta_1) | \epsilon_n^{i\alpha}(\eta_2) \rangle$ describes the degree of correlation between mode m at strain η_1 and mode n at strain η_2. We expect $\sum_m |p_{mn}|^2 = 1$, which is indeed confirmed by our numerical calculations. From the quantity p_{mn}, one can identify the correspondences and evolutions between modes at different strains. The correspondences are depicted by the connecting lines in Fig. 1. Furthermore, p_{mn} is also very useful in examining the strain-induced intermode mixing when it does occur.

Figure 1 reveals that the mode sequence in strained $BaTiO_3$ drastically differs from the unstrained case. This drastic difference occurs even for a moderate strain at $\eta = -2.5\%$. The key distinctions between mode sequences at $\eta = -2.5\%$ and at $\eta = 0$ are as follows: (i) At $\eta = -2.5\%$, the frequency of $A_1(TO_2)$ is notably above those of $E(TO_3)$, $E(LO_2)$, and B_1. This clearly is not the case at $\eta = 0\%$, where the former mode is well below the latter three modes. (ii) $A_1(LO_3)$ and $E(LO_4)$ undergo a crossover in frequency as strain varies. At $\eta = 0$, $A_1(LO_3)$ is the mode with the highest frequency. However, at $\eta = -2.5\%$, $E(LO_4)$ exhibits the highest frequency. (iii) Interestingly, $E(TO_3)$, $E(LO_2)$, and B_1 modes are very close in frequency at $\eta = 0$, but they are well separated in sequence at $\eta = -2.5\%$. (iv) Obviously, the hardening of the soft mode $E(TO_1)$, which crosses with $A_1(TO_1)$, $E(TO_2)$, $E(LO_1)$, and $A_1(LO_1)$, also contributes substantially to the change in mode sequence. Furthermore, as pointed out by Choudhury *et al.*, the zone-center phonons in unstrained perovskites exhibit interesting frequency gaps [46]. These phonon gaps may have innovative applications in sound and heat revolutions [47]. The phonon-frequency gaps are confirmed by the $\eta = 0$ calculations in Fig. 1 in the frequency ranges of 200–300, 300–450, and 500–670 cm^{-1}. These phonon gaps largely disappear or are significantly reduced at strain $\eta = -3.3\%$, however.

The theoretical results have important implication for experiments. They reveal that, in Raman and/or infrared experiments, using the mode sequence of unstrained $BaTiO_3$ to index the spectroscopy peaks observed in epitaxially strained $BaTiO_3$ may lead to significant errors. Specifically, when $BaTiO_3$ is strained to the $SrTiO_3$ substrate (with about 2.5% compressive strain), the mode sequence is very different from that in unstrained $BaTiO_3$, as shown in Fig. 1. We instead need to use the correct mode sequence (e.g., the one in Fig. 1) to assign experimentally measured peaks.

B. Strain-induced large-frequency shifts for nonsoft modes

Strain-dependent frequency shift, defined as $\Delta\omega_n(\eta) = \omega_n(\eta) - \omega_n(\eta = 0)$ for a given mode n, is depicted in Fig. 2. Note that determination of $\Delta\omega_n(\eta)$ is possible only after the correspondences between modes at different strains have been mapped out. According to the magnitude and sign of $\Delta\omega$, the frequency responses in Fig. 2 can be categorized into three groups: large increase ($\Delta\omega > 50$ cm^{-1}), moderate increase ($0 < \Delta\omega < 50$ cm^{-1}), and frequency decrease $\Delta\omega < 0$ when η varies in the considered strain range from 0% to −3.3%.

Interestingly, $A_1(TO_2)$, $E(LO_4)$, $A_1(TO_3)$, and $E(TO_4)$ in Fig. 2 all display a large strain-induced frequency shift, with $\Delta\omega > 50$ cm^{-1} at $\eta = -3.3\%$. Particularly, $A_1(TO_2)$ increases its frequency by more than 140 cm^{-1} at $\eta = -3.3\%$ with respect to $\eta = 0$, which is rather phenomenal. Note that none of the above modes are soft modes. Also, notably, unlike most other modes, B_1 shows an unusual frequency decrease in Fig. 2.

Results in Fig. 2 defy the common wisdom. According to symmetry, vibrations in perovskites of tetragonal structure can be either along the in-plane directions (e.g., the E modes), with frequency denoted as $\omega_\parallel$, or along the out-of-plane direction (e.g., the A_1 modes), with frequency denoted as $\omega_\perp$. When a compressive strain is applied, one would think that $\omega_\parallel$ would increase since along the in-plane directions atomic interaction is strengthened by the strain. Meanwhile, along the out-of-plane direction, interatomic interaction is weakened, and hence a decrease in $\omega_\perp$ is expected. However, the calculation results in Fig. 2 reveal different conclusions. In fact, upon the impose of strain, $A_1(TO_2)$, $A_1(TO_3)$, and $A_1(LO_3)$ in Fig. 2 all increase their $\omega_\perp$ frequencies very substantially, in sharp contrast to the common belief. Furthermore, note the subtle decrease in the $\omega_\parallel$ frequency for $E(LO_3)$, which also deviates

from the above common thinking. The direct first-principles calculations suggest a different mechanism that dictates the mode's frequency response.

Our calculations are consistent with and provide an explanation for experimental observations. In the UV Raman experiments, when a $(BaTiO_3)_5/(SrTiO_3)_4 \times 25$ superlattice is epitaxially strained to a $SrTiO_3$ substrate, the nonsoft TO_4 mode of $BaTiO_3$ is shifted from 486 cm^{-1} in bulk to 540 cm^{-1} in the strained superlattice [1]. According to Fig. 2, when $BaTiO_3$ is strained to $SrTiO_3$ at $\eta = -2.5\%$, the $E(TO_4)$ frequency increases by 45 cm^{-1}. This is in good agreement with the experiment, where a shift of 54 cm^{-1} was observed [1]. Moreover, our theory predicts that there are other nonsoft modes such as $A_1(TO_2)$, $E(LO_4)$, and $A_1(TO_3)$ that are subjected to even larger shifts (see Fig. 2).

The physical origin underlying the mode behaviors in Fig. 2 is rather simple and can be explained by the relative motion between Ti and O along the direction of vibration. When Ti and O vibrate oppositely or when Ti does not vibrate but O vibrates toward Ti, the frequency increases with strain, which is indeed the case for the Slater modes $A_1(TO_2)$ and $E(LO_4)$ and for the Axe modes $A_1(TO_3)$ and $E(TO_4)$ (the displacement patterns of these modes are given in the Appendix). On the other hand, for modes in which Ti and O atoms vibrate in the same direction, the frequencies moderately change, such as the Last modes $E(TO_2)$ and $E(LO_1)$. For the B_1 mode, the vibration largely weakens the atomic interaction along the out-of-plane direction, leading to a frequency decrease.

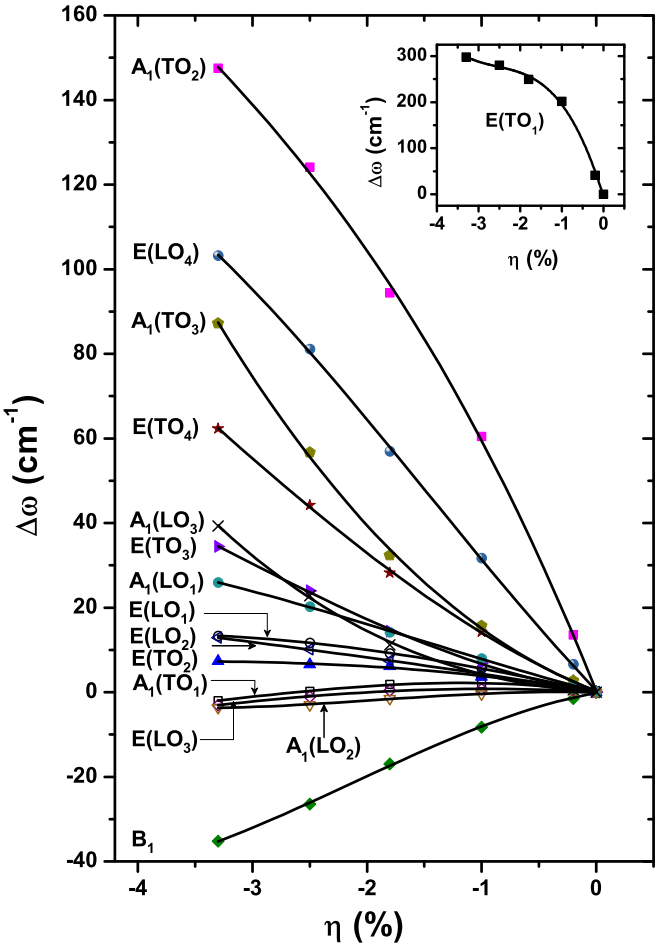

FIG. 2. (Color online) Frequency shift $\Delta\omega$ as a function of strain. In the inset, the frequency shift for soft mode $E(TO_1)$ is shown.

Another interesting observation in Fig. 2 is that $\Delta\omega$ is nonlinear as a function of strain for $A_1(TO_2)$, $A_1(TO_3)$, and $A_1(LO_3)$, while for other modes it is fairly linear. The nonlinearity has important consequences for the strain-mode coupling. To see this, we start with a simple model and write the energy as $E = \frac{1}{2}m\omega^2(\eta)Q^2$, where Q is the normal mode and $\omega(\eta)$ is strain dependent. Consider the strain dependence of ω as $\omega(\eta) = \omega_0 + \alpha_1\eta + \alpha_2\eta^2$. It is straightforward to prove that, if ω depends linearly on η, i.e., $\alpha_2 = 0$, the strain-coupling terms include only ηQ^2 and $\eta^2 Q^2$. But when the nonlinear effect is important, i.e., α_2 cannot be neglected, the strain-mode coupling should also include the $\eta^3 Q^2$ term.

Furthermore we analyze how the polarization vector (i.e., mode eigenvector $|\epsilon_n^{i\alpha}\rangle$) changes with strain η, where n is the mode index, i is the atom index, and α is the vibration-direction index. We find that some modes do not change their polarization vectors appreciably, such as $E(LO_1)$. The $E(LO_1)$ mode vibrates along the x direction, and we only need to give the nonzero x components of polarization vector. $|\epsilon_n^{Ba,x}, \epsilon_n^{Ti,x}, \epsilon_n^{O1,x}, \epsilon_n^{O2,x}, \epsilon_n^{O3,x}\rangle$ of $E(LO_1)$ is found to be $(0.627, -0.675, -0.183, -0.243, -0.243)$ at $\eta = 0$, $(0.627, -0.676, -0.216, -0.206, -0.246)$ at $\eta = -1.8\%$, and $(0.625, -0.679, -0.241, -0.166, -0.250)$ at $\eta = -3.3\%$, showing only small changes. On the other hand, some modes [e.g., $A_1(TO_2)$, $E(TO_4)$, and $A_1(TO_3)$] have quite large changes in the polarization vector, and the polarization vectors of these modes are given in Table III, showing that the O (and/or Ti) components vary significantly with strain. We further find that the large change in the polarization vector correlates well with and is responsible for the nonlinear strain dependence of $\Delta\omega$. For instance, the eigenvector (particularly, the Ti component) of $A_1(TO_3)$ changes substantially with strain, which leads to the strong nonlinearity in $\Delta\omega$.

C. LO-TO splitting

We begin by rigorously defining the LO-TO splitting, which will serve as the foundation for the present study of this important quantity. Let $\{|\epsilon'_n\rangle, \omega'_n(\mathbf{q} \to 0)\}$ be the mode eigenvectors and eigenvalues obtained from the diagonalization of the total dynamic matrix $D = D^a(\mathbf{q} = 0) + D^{na}(\mathbf{q} \to 0)$, where $D_{ij}^{\alpha\beta} = \frac{1}{\sqrt{M_i M_j}} C_{ij}^{\alpha\beta}$ includes both the analytic and nonanalytic contributions, thereby taking into account the effects caused by the displacement-induced electric field. Let $\{|\epsilon_n\rangle, \omega_n(\mathbf{q} = 0)\}$ be the eigenvectors and eigenvalues obtained from only the analytic $D^a(\mathbf{q} = 0)$, and therefore the displacement-induced electric field and the LO-TO splitting are not accounted for.

It should be emphasized that knowing the frequencies $\{\omega'_n(\mathbf{q} \to 0)\}$ and $\{\omega_n(\mathbf{q} = 0)\}$ of individual modes does not mean knowing the LO/TO splitting. As we previously described in the Introduction, one cannot naively define the LO-TO splitting as the simple difference between *one* frequency $\omega'_i(\mathbf{q} \to 0)$ and *another* frequency $\omega_j(\mathbf{q} = 0)$. This naive approach is fundamentally incorrect because one LO mode often comes from multiple TO modes and all of these

TABLE III. Evolution of selected phonon eigenvectors with the η strain in tetragonal $BaTiO_3$. The selected modes possess noticeable change in the individual components at higher strains. The vibration direction is indicated in the first column by an italic letter inside parentheses below the mode name. O2 is the apical oxygen atom beneath Ti along the tetragonal c axis.

		Eigenvector components		
Modes	Atoms	$\eta = 0$	$\eta = -1.8\%$	$\eta = -3.3\%$
$E(TO_1)$	Ba	0.020	0.081	−0.078
(y)	Ti	0.677	0.611	0.694
	O1	−0.358	−0.584	−0.661
	O2	−0.308	−0.244	−0.040
	O3	−0.564	−0.468	−0.271
$A_1(TO_2)$	Ba	−0.190	−0.089	−0.085
(z)	Ti	0.835	0.766	0.715
	O1	−0.270	−0.422	−0.491
	O2	−0.348	−0.223	−0.007
	O3	−0.270	−0.422	−0.491
$E(TO_4)$	Ba	−0.011	−0.002	0.001
(y)	Ti	0.142	0.025	−0.091
	O1	−0.478	−0.456	−0.431
	O2	−0.467	−0.384	−0.269
	O3	0.730	0.803	0.856
$A_1(TO_3)$	Ba	−0.009	−0.002	0.008
(z)	Ti	0.052	−0.115	−0.288
	O1	−0.429	−0.335	−0.216
	O2	0.794	0.874	0.908
	O3	−0.429	−0.335	−0.216

TO modes have nearly equal contributions due to the inevitable strong intermode mixing caused by the long-range Coulomb interaction. Further, it is also worth pointing out that in the Lyddane-Sachs-Teller (LST) relation and optical sum rules, it is the frequencies $\{\omega\prime_n(\mathbf{q}\to 0)\}$ and $\{\omega_n(\mathbf{q}=0)\}$, not the LO-TO *splittings*, that enter the formulas [48]. In fact, the LO-TO splitting has not been rigorously defined, to the best of our knowledge.

We now describe our scheme. Since $\{|\epsilon_m\rangle\}$ form a complete basis for any mode at $\mathbf{q}=\mathbf{0}$, it is hence always possible to write $|\epsilon\prime_n\rangle = \sum_m \alpha_{mn}|\epsilon_m\rangle$. Due to the strong mixing among different modes caused by the displacement-induced electric field, there is more than one dominant contribution in the above summation over m. In other words, α_{mn} are often large and significant for multiple m modes. One can define new frequencies as

$$\widetilde{\omega}_n^2 = \sum_m |\,\alpha_{mn}\,|^2\,\omega_m^2\,, \tag{3}$$

bearing in mind that the dynamic eigenstate equation is $D|\epsilon_m\rangle = \omega_m^2|\epsilon_m\rangle$, not $D|\epsilon_m\rangle = \omega_m|\epsilon_m\rangle$. $\widetilde{\omega}_n$ in Eq. (3) properly accounts for the mode mixing when multiple TO modes contribute to form a LO phonon, and meanwhile, all frequencies in this equation are without LO-TO splittings. The LO-TO splitting $\Delta\omega_n^{LT}$ is then defined as

$$\Delta\omega_n^{LT} = \omega\prime_n(\mathbf{q}\to 0) - \widetilde{\omega}_n(\mathbf{q}=0)\,, \tag{4}$$

by which one can calculate $\Delta\omega_n^{LT}$ for arbitrary mode $|\epsilon\prime_n\rangle$.

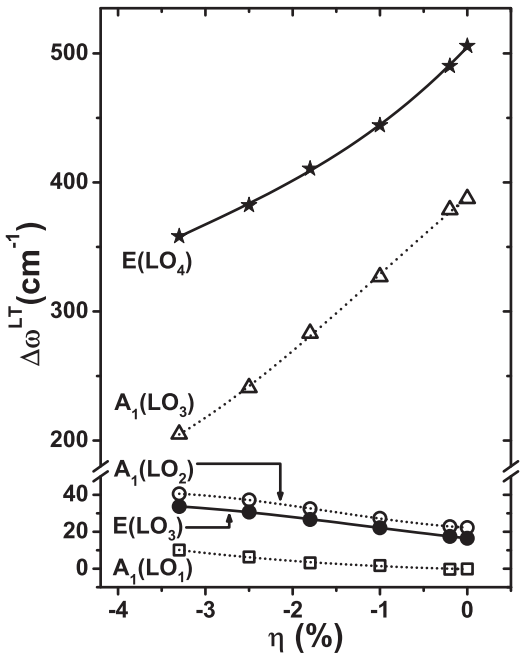

FIG. 3. The LO-TO splittings $\Delta\omega^{LT}$ as a function of strain for modes with sizable splittings.

Equations (3) and (4) provide an approach to determine and quantitatively study LO-TO splittings. The advantages of this approach are as follows: (i) It properly accounts for the electric-field-induced strong mode mixing. (ii) With this formula, the LO-TO splitting can now be quantitatively calculated for any $|\epsilon\prime_n\rangle$ mode. (iii) It allows us to find whether there are LO modes other than $E(LO_4)$ that may display a large LO-TO splitting. (iv) By using the approach, we can find out how the LO-TO splitting quantitatively changes with strain, which should work for a wide class of ferroelectric materials.

Using the above approach and formulas, we numerically find that $\Delta\omega_n^{LT}$ is significant only for the LO modes, as it should be. To give us more insight, Fig. 3 depicts the LO-TO splittings for the LO modes with significant $\Delta\omega^{LT}$. In Fig. 3, $\mathbf{q}$ approaches the zone center along the [001] direction for A(LO) modes and along the [100] direction for E(LO) modes.

While soft modes in ferroelectrics, such as $E(TO_1)$ in $BaTiO_3$, are known to interact strongly with the displacement-induced electric field and to generate a giant LO-TO splitting in forming the $E(LO_4)$ mode, the quantitative understanding of LO-TO splitting for *other modes* is virtually unknown. Interestingly, Fig. 3 reveals that $E(LO_4)$ is not the only mode that displays a large LO/TO splitting. Rather remarkably, $\Delta\omega_n^{LT}$ of $A_1(LO_3)$ is nearly as large as that of $E(LO_4)$. This is phenomenal since, unlike $E(LO_4)$, $A_1(LO_3)$ does not originate from a soft mode.

Furthermore, Fig. 3 shows quantitatively that the LO/TO splittings in ferroelectric $BaTiO_3$ change in an approximately linear manner with the strain. More specifically, with the increase of compressive strain, $\Delta\omega_n^{LT}$ decreases sharply for $E(LO_4)$ and $A_1(LO_3)$ modes.

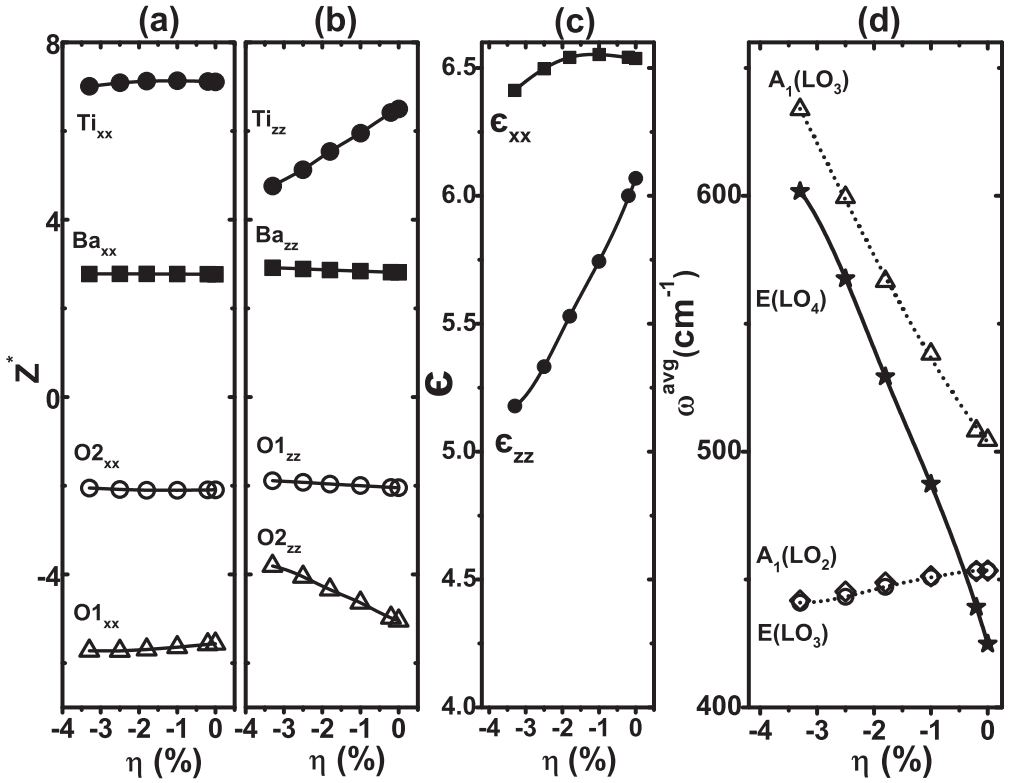

FIG. 4. Changes of the following quantities as a function of strain in $BaTiO_3$: (a) the Z^*_{xx} component of the Born effective charge, (b) the Z^*_{zz} component of the Born effective charge, (c) the high-frequency dielectric constants ϵ^{∞}_{xx} and ϵ^{∞}_{zz}, and (d) the average ω^{avg} for $E(LO_4)$ and $A_1(LO_3)$ modes.

The dramatic decrease of the LO-TO splitting with strain for $E(LO_4)$ and $A_1(LO_3)$ cannot be naively explained by the Born effective charge Z^* and the dielectric constant $\boldsymbol{\epsilon}^{\infty}$; the latter two quantities are shown in Figs. 4(a)–4(c). Take $E(LO_4)$ as an example. The $E(LO_4)$ modes vibrate along the in-plane directions. However, the in-plane component Z^*_{xx} almost does not change for all atoms [Fig. 4(a)], and ϵ^{∞}_{xx} does not change much either [Fig. 4(c)]. Consequently, the nonanalytic $D^{\alpha\beta,na}_{ij}$ contribution is nearly a constant independent of strain for the $E(LO_4)$ mode, which cannot explain the drastic decrease of the LO-TO splitting for this mode. We find that the declining $\Delta\omega^{LT}$ is due to the increase of the average frequency, defined as

$$\omega^{\text{avg}}_n = \frac{\omega\prime_n(\mathbf{q}\to 0) + \widetilde{\omega}_n(\mathbf{q}=0)}{2}. \tag{5}$$

Using ω^{avg}_n, the LO-TO splitting can be written as $\Delta\omega^{LT}_n = \frac{1}{2\omega^{\text{avg}}_n}\sum_i \frac{4\pi}{\Omega M_i} e^2 \frac{(\mathbf{q}\cdot\mathbf{Z}^*_i)(\mathbf{q}\cdot\mathbf{Z}^*_i)}{\mathbf{q}\cdot\boldsymbol{\epsilon}^{\infty}\cdot\mathbf{q}}$; that is, $\Delta\omega^{LT}_n$ is inversely proportional to ω^{avg}_n. Figure 4(d) shows the average frequency ω^{avg}_n for $E(LO_4)$ and $A_1(LO_3)$. We see that, when η varies from 0% to −3.3%, ω^{avg}_n increases considerably for both modes, leading to the significant decrease of the LO-TO splitting. Therefore it is ω^{avg}_n that governs the strain dependence of the LO-TO splitting in perovskite ferroelectrics.

IV. SUMMARY

Mode sequence is of key relevance in properly assigning spectroscopic peaks. In this study, several interesting changes in mode sequence were determined and revealed in strained $BaTiO_3$ by density functional perturbation calculations; these changes are caused by the intrinsic strain-induced mode crossing and intermode mixing. Furthermore, the frequency shifts of individual zero-center phonons were mapped out and compared to experiments, with particular attention given to those nonsoft modes. A group of nonsoft modes with a sensitive strain-dependent frequency were identified. Moreover, the LO-TO splitting is rigorously defined, which allows this important physical quantity to be quantitatively studied. We further revealed which mode other than $E(LO_4)$ displays strong LO-TO splitting and how the splitting depends on the epitaxial strain. Our specific findings are summarized in the following.

(i) The mode sequence is widely different at $\eta = -2.5\%$ than at zero strain. The changes in mode sequence stem from multiple mode crossings. At $\eta = -2.5\%$, the highest mode is $E(LO_4)$, not $A_1(LO_3)$. Also, unlike the unstrained $BaTiO_3$ in which $A_1(TO_2)$ is well below $E(TO_3)$, $E(LO_2)$, and B_1, at high strain $A_1(TO_2)$ surpasses all of them. Furthermore, the characteristic phonon gaps at zero strain largely disappear at high strains. Our calculations quantitatively predict the magnitude of strain at which one mode crosses the others (see Fig. 1).

(ii) Large strain-induced frequency shifts were shown to occur, even for nonsoft phonons. As shown in Fig. 2, these nonsoft modes include $A_1(TO_2)$, $E(LO_4)$, $A_1(TO_3)$, and $E(TO_4)$. Indeed, large shift has been observed in experiments using the new UV Raman spectroscopy [1]. At $\eta = -2.5\%$, the

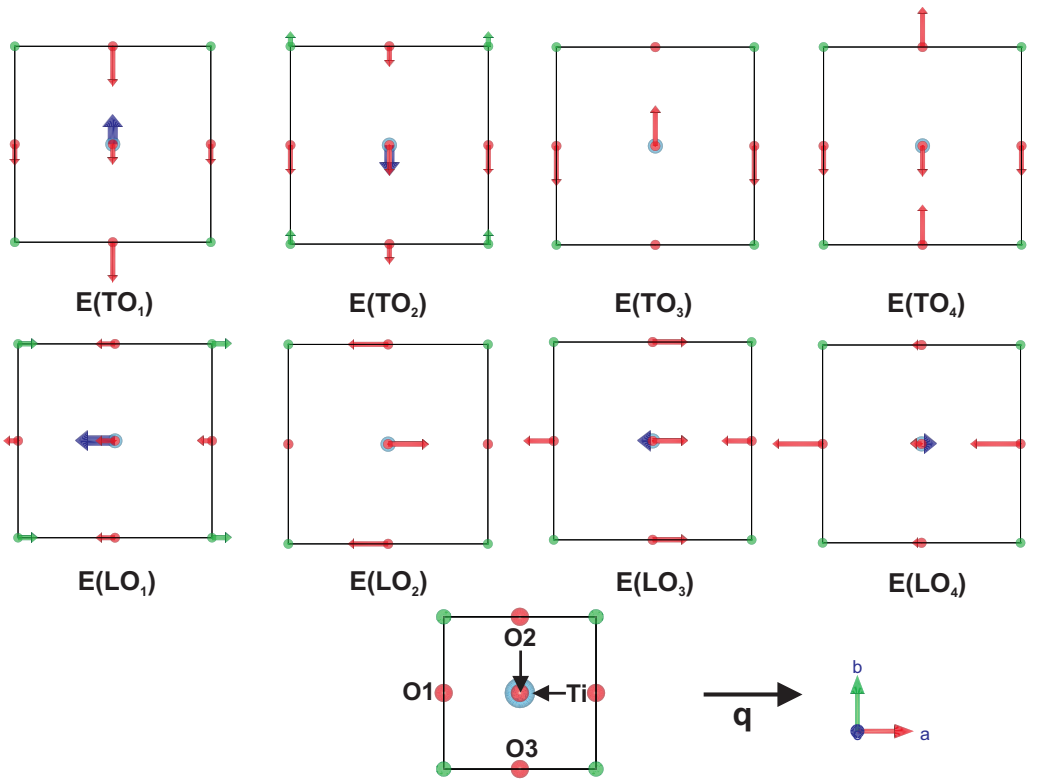

FIG. 5. (Color online) Top view (i.e., from the **-c** axis) of phonon displacements of the E modes in unstrained $BaTiO_3$. The axes in the bottom-right corner refer to the crystallographic axes {**a**, **b**, **c**}, coinciding with the Cartesian {**x**, **y**, **z**} directions, respectively. **q** approaches the zone center along the [100] direction for E(LO) modes. The green, light blue, and red spheres represent Ba, Ti, and O atoms, respectively. Atoms are labeled at the bottom of the figure. The arrows on atoms represent the magnitude of displacement; the dark blue arrow is for Ti atom to differentiate its displacement from that of the O2 atom along the same line of view.

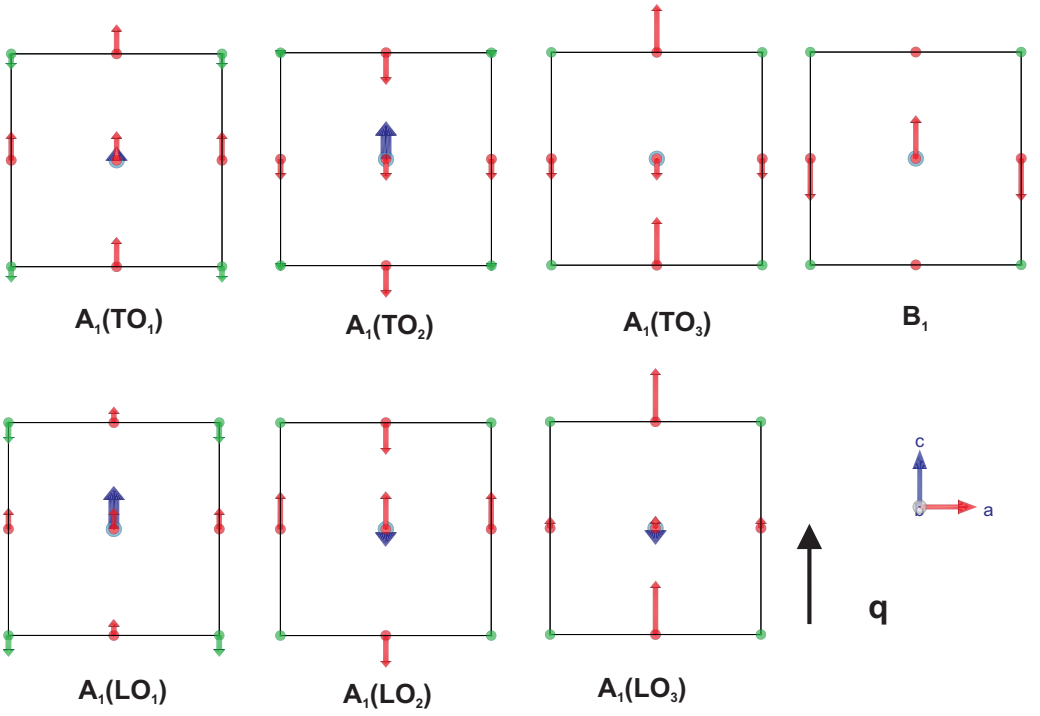

FIG. 6. (Color online) Side view (i.e., from the **b** axis) of phonon displacements of A_1 and B_1 modes in unstrained $BaTiO_3$. The axes in the lower-right corner refer to the crystallographic axes. **q** approaches the zone center along the [001] direction for A_1(LO) modes.

theoretical shift of 45 cm^{-1} for $E(TO_4)$ is in good agreement with the measured value of 54 cm^{-1} in experiment. Note that our theory predicts that $E(TO_4)$ is only one of the nonsoft modes displaying large strain-induced frequency change; the frequency shifts of other three nonsoft modes are even larger (see Fig. 2).

Our calculations in Fig. 2 further reveal that, while frequency shift $\Delta\omega$ linearly depends on strain for most modes, there are interesting exceptions; that is, strong nonlinear dependency is found for modes $A_1(TO_3)$ and $A_1(LO_3)$, caused by considerable changes in the phonon eigenstates. This nonlinear dependence implies that the $\eta^3 Q^2$ term cannot be neglected in the formulation of the strain-mode coupling.

(iii) The rigorous definition of the LO-TO splitting enables the discovery of new physics. A markedly large LO-TO splitting is found for the $A_1(LO_3)$ mode, in addition to the well-known $E(LO_4)$. We further showed that the LO-TO splittings of $A_1(LO_3)$ and $E(LO_4)$ decrease sharply with the increasing compressive strain, showing a rather linear dependence. The decline of the LO-TO splitting cannot be explained by the effective charge and high-frequency dielectric constant and is instead due to the large change in the average frequency ω_n^{avg}.

Considering that ultraviolet Raman spectroscopy is now available in experiments [1–3] and considering that nonsoft modes may play a pivotal role in determining the structure properties in ferroelectrics as demonstrated in Ref. [49], we hope that our study will stimulate further theoretical and experimental interest in mode sequence, the behaviors of nonsoft modes, and the quantitative understanding of LO-TO splitting.

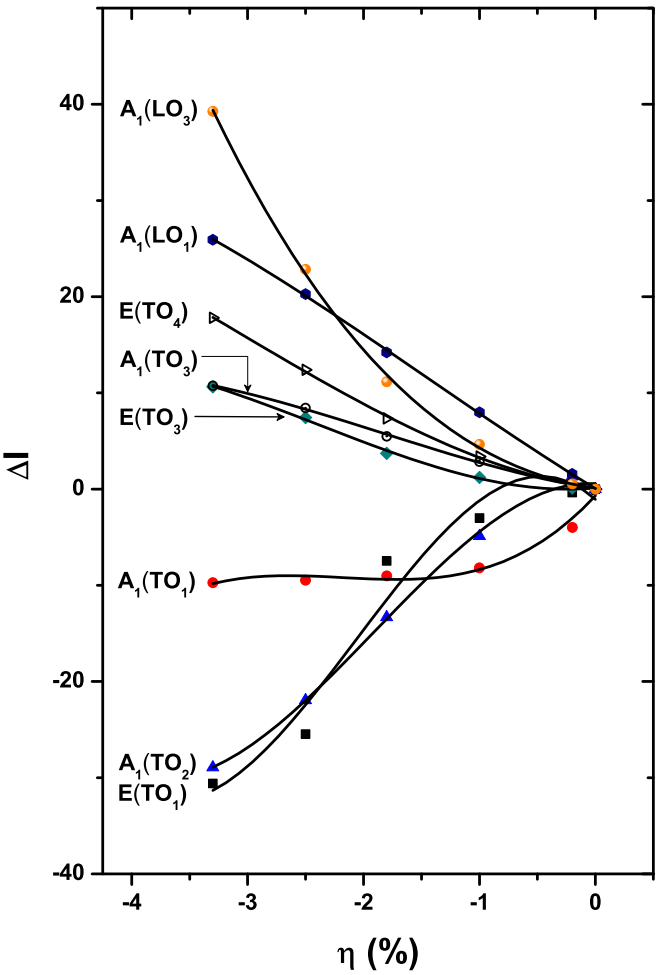

FIG. 7. (Color online) Changes in infrared intensity as a function of strain for modes that display noticeable intensity variation.

ACKNOWLEDGMENT

This work was supported by the Office of Naval Research.

APPENDIX

This Appendix provides additional results that include the vibration displacements and IR intensities of the zone-center modes. Vibration displacements are of key relevance in terms of understanding the behaviors of individual modes and are given in Fig. 5 for all E modes and in Fig. 6 for all A_1 modes in unstrained $BaTiO_3$. We choose the top view (i.e., the view from the -**c** axis) for the E modes since they vibrate on the **ab** plane. Meanwhile, we choose the side view (i.e., the view from the **b** axis) for the A_1 modes since these modes vibrate along the **c** axis.

IR spectroscopy is an important technique that probes the change in the dipole moment due to lattice vibration, namely, the infrared intensity $I \propto |\frac{\partial \mathbf{P}}{\partial \mathbf{Q}}|^2$, where $\mathbf{Q}$ is the normal mode amplitude. This results in [50]

$$I = \sum_{\alpha} \left| \sum_{s\beta} Z_s^{*\alpha\beta} u_s^{\beta} \right|^2, \tag{A1}$$

where u_s^{β} is the displacement of atom s in the β direction. When normal modes alter with strain, the change in IR intensity may also be detected.

From the group-theory analysis, all modes except B_1 in $BaTiO_3$ of $P4mm$ symmetry are {IR + R} active, while the B_1 mode is only Raman active. The change in IR intensity, $\Delta I_n(\eta) = I_n(\eta) - I_n(\eta = 0)$, is depicted in Fig. 7 for different modes as a function of strain. Intensities of $E(TO_1)$ and $A_1(TO_2)$ decrease with strain, while those of $A_1(LO_3)$, $A_1(LO_1)$, and $E(TO_4)$ increase. The behaviors of the IR intensities in Fig. 7 can be largely explained by the strain dependence of the effective charges [Figs. 4(a) and 4(b)] and displacements (Table III) according to Eq. (A1). For $A_1(TO_2)$, which vibrates along the c axis, $|Z_{zz}^*|$ decreases for both Ti and O2 [Fig. 4(b)], and displacements of these two atoms also decrease, leading to the declining IR intensity. For $E(TO)$ modes, since Z_{xx}^* does not change much upon the strain [Fig. 4(a)], the change in IR intensity is mainly due to the displacement change. For instance, for the $E(TO_4)$ mode, the increase in its IR intensity comes largely from the increase in the O3 displacement (Table III).

[1] D. Tenne *et al.*, Science **313**, 1614 (2006).

[2] D. A. Tenne, P. Turner, J. D. Schmidt, M. Biegalski, Y. L. Li, L. Q. Chen, A. Soukiassian, S. Trolier-McKinstry, D. G. Schlom, X. X. Xi, D. D. Fong, P. H. Fuoss, J. A. Eastman, G. B. Stephenson, C. Thompson, and S. K. Streiffer, Phys. Rev. Lett. **103**, 177601 (2009).

[3] D. A. Tenne, A. K. Farrar, C. M. Brooks, T. Heeg, J. Schubert, H. W. Jang, C. W. Bark, C. M. Folkman, C. B. Eom, and D. G. Schlom, Appl. Phys. Lett. **97**, 142901 (2010).

[4] P. Y. Yu and M. Cardona, *Fundamentals of Semiconductors Physics and Materials Properties* (Springer, Berlin, 2001).

[5] U. D. Venkateswaran, V. M. Naik, and R. Naik, Phys. Rev. B **58**, 14256 (1998), and references therein.

[6] R. Yu and H. Krakauer, Phys. Rev. Lett. **74**, 4067 (1995).

[7] D. J. Singh, Phys. Rev. B **53**, 176 (1996).

[8] Ph. Ghosez, E. Cockayne, U. V. Waghmare, and K. M. Rabe, Phys. Rev. B **60**, 836 (1999).

[9] C. Bungaro and K. M. Rabe, Phys. Rev. B **65**, 224106 (2002).

[10] I. I. Naumov and H. Fu, Phys. Rev. B **72**, 012304 (2005).

[11] X. Wang and D. Vanderbilt, Phys. Rev. B **74**, 054304 (2006).

[12] A. Garcia and D. Vanderbilt, Phys. Rev. B **54**, 3817 (1996).

[13] M. Born and K. Huang, *Dynamical Theory of Crystal Lattices* (Oxford University Press, Oxford, 1954).

[14] R. A. Cowley, Adv. Phys. **29**, 1 (1980).

[15] M. E. Lines and A. M. Glass, *Principles and Applications of Ferroelectrics and Related Materials* (Clarendon, Oxford, 1979).

[16] M. Dawber, K. M. Rabe, and J. F. Scott, Rev. Mod. Phys. **77**, 1083 (2005).

[17] C. H. Ahn, K. M. Rabe, and J. M. Triscone, Science **303**, 488 (2004).

[18] A. S. Mischenko, Q. Zhang, J. F. Scott, R. W. Whatmore, and N. D. Mathur, Science **311**, 1270 (2006); J. F. Scott, Annu. Rev. Mater. Res. **41**, 229 (2011).

[19] K. Uchino, *Piezoelectric Actuators and Ultrasonic Motors* (Kluwer Academic, Boston, 1996).

[20] S.-E. Park and T. R. Shrout, J. Appl. Phys. **82**, 1804 (1997).

[21] A. Garcia and D. Vanderbilt, Appl. Phys. Lett. **72**, 2981 (1998).

[22] H. Fu and R. E. Cohen, Nature (London) **403**, 281 (2000).

[23] X. Fu, I. I. Naumov, and H. Fu, Nano. Lett. **13**, 491 (2013).

[24] J. F. Scott, *Ferroelectric Memories* (Springer, Berlin, 2000).

[25] R. E. Cohen, Nature (London) **358**, 136 (1992).

[26] R. E. Cohen and H. Krakauer, Phys. Rev. B **42**, 6416 (1990).

[27] R. D. King-Smith and D. Vanderbilt, Phys. Rev. B **47**, 1651 (1993).

[28] R. Resta, Rev. Mod. Phys. **66**, 899 (1994).

[29] L. D. Landau and E. M. Lifshitz, *Statistical Physics* (Pergamon, New York, 1980), Part 1.

[30] I. I. Naumov, L. Bellaiche, and H. Fu, Nature (London) **432**, 737 (2004); I. Naumov and H. Fu, Phys. Rev. Lett. **98**, 077603 (2007).

[31] A. S. Barker, Jr., Phys. Rev. **136**, A1290 (1964).

[32] W. Zhong, R. D. King-Smith, and D. Vanderbilt, Phys. Rev. Lett. **72**, 3618 (1994).

[33] Ph. Ghosez, J.-P. Michenaud, and X. Gonze, Phys. Rev. B **58**, 6224 (1998).

[34] P. Hohenberg and W. Kohn, Phys. Rev. **136**, B864 (1964); W. Kohn and L. J. Sham, *ibid.* **140**, A1133 (1965).

[35] P. Giannozzi *et al.*, J. Phys. Condens. Matter **21**, 395502 (2009).

[36] QUANTUM ESPRESSO, http://www.quantum-espresso.org.

[37] N. Troullier and J. L. Martins, Phys. Rev. B **43**, 1993 (1991).

[38] H. Fu and O. Gulseren, Phys. Rev. B **66**, 214114 (2002); A. Raeliarijaona and H. Fu, J. Appl. Phys. **115**, 054105 (2014).

[39] R. Wahl, D. Vogtenhuber, and G. Kresse, Phys. Rev. B **78**, 104116 (2008).

[40] S. Baroni, S. de Gironcoli, A. Dal Corso, and P. Giannozzi, Rev. Mod. Phys. **73**, 515 (2001).

[41] S. Baroni, P. Giannozzi, and A. Testa, Phys. Rev. Lett. **58**, 1861 (1987).

[42] X. Gonze, Phys. Rev. A **52**, 1096 (1995).

[43] X. Gonze and C. Lee, Phys. Rev. B **55**, 10355 (1997).

[44] P. Hermet, M. Veithen, and Ph. Ghosez, J. Phys.: Condens. Matter **21**, 215901 (2009).

[45] R. A. Evarestov and A. V. Bandura, J. Comput. Chem. **33**, 1123 (2012).

[46] N. Choudhury, E. J. Walter, A. I. Kolesnikov, and C.-K. Loong, Phys. Rev. B **77**, 134111 (2008).

[47] M. Maldovan, Nature (London) **503**, 209 (2013).

[48] R. H. Lyddane, R. G. Sachs, and E. Teller, Phys. Rev. **59**, 673 (1941).

[49] J. M. Perez-Mato, M. Aroyo, A. Garcia, P. Blaha, K. Schwarz, J. Schweifer, and K. Parlinski, Phys. Rev. B **70**, 214111 (2004).

[50] D. Porezag and M. R. Pederson, Phys. Rev. B **54**, 7830 (1996).